First-principles calculation of the electron-phonon interaction in semiconductor nanoclusters

Peng Han and Gabriel Bester*
Max-Planck-Institut für Festkörperforschung, Heisenbergstraße 1, D-70569 Stuttgart, Germany
(Received 10 April 2012; published 8 June 2012)

We present a first-principles density functional theory approach to study the electron-phonon coupling of semiconductor nanoclusters using the self-consistent change of the potential caused by a frozen-phonon distortion of the lattice. This approach has been examined by comparing the results with *ab initio* linear-response calculation and allows us to study the electron-phonon coupling of nanoclusters with radii up to 16 Å (around 1000 atoms) at the level of density functional perturbation theory. We further study the electronic relaxation processes between discrete electronic states of silicon nanoclusters through coupling to the lattice and compare our results with experiments. An increase of electron-phonon coupling strength with decreasing cluster size is obtained from our calculation. We also find that the absorption and emission of vibrons leads to an ultrafast (femtosecond) oscillation in the occupation probability of the excited electronic state given by the electron-phonon coupling. The envelope function of the occupation probability decays exponentially due to the phonon lifetime (around picosecond) and potentially the electron trapping (around picosecond) of surface states.

DOI: 10.1103/PhysRevB.85.235422 PACS number(s): 63.22.Kn, 71.38.−k, 73.22.Dj

I. INTRODUCTION

Colloidal semiconductor nanoclusters (NCs) or quantum dots have attracted considerable attention in optoelectronics, spintronics, photovoltaic, and biolabeling due to their size-tunable electronic and optical properties.[1–9] The modification of the electronic and optical properties induced by changes in their size or morphology are rather well understood theoretically and controlled experimentally. One open problem in nanostructure science is the effects of temperature on the electronic and optical properties. This topic is important for real world applications where temperature broadening, relaxation of charge carriers, and loss of quantum coherence[3,7,10,11] are often limiting factors. In order to address temperature effects, where vibrations are naturally involved, a solid understanding of the electron-phonon (e-ph) interaction in NCs is decisively required. Strictly speaking, the concept of phonon is only defined for bulk systems, and is no longer well defined in quantum dots with three-dimensional (3D) confinement. The phonons from the bulk with their well-studied dispersions collapse into discrete vibrational states, or called vibrons in NCs.[12]

The e-ph interaction has been the subject of theoretical investigation since the middle of the last century.[13] Following the pioneering investigations of phenomenological deformation potentials, piezoelectric potentials, and Fröhlich interactions on the base of continuum models,[13,14] the atomistic methods such as the frozen-phonon approach[15–19], *ab initio* density functional perturbation theory (DFPT),[20–25] and Born-Oppenheimer molecular dynamics (BOMD)[26,27] have been proposed to study the e-ph interaction. Among these methods, *ab initio* DFPT calculations represent the state-of-the-art and provide accurate e-ph coupling information. BOMD simulations, which monitor the change in the electronic levels under the influence of vibrations, can in principle describe the e-ph interaction beyond the harmonic approximation. However, both of these accurate first-principles methods are currently only possible for bulk and very small NCs due to the high computational demand.

In contrast to DFPT, where the change of potential is treated as the linear response of the charge density to the atomic displacement, the frozen-phonon approach is a direct method for the calculation of e-ph coupling. In this approach, the perturbation of specific phonon modes on the electronic states are handled through a frozen atomic displacement pattern.[15–17] The frozen-phonon approach was initially proposed as a method for the calculation of bulk phonon frequencies.[28,29] In this approach, the total energy of a system is obtained for a specific atomic displacement pattern according to the phonon eigenmode. The phonon frequency is then calculated from energy difference between the system with and without the atomic displacement. In this approach, the computation of long wavelength bulk phonon frequencies is limited by the size of the cell. Since the DFPT linear-response approach provides accurate results of the phonon eigenmode with low computational demand,[30] the frozen-phonon method is rarely applied to calculate the phonon frequency now. With the development of first-principles calculation, the frozen-phonon approach was extended to self-consistent calculations of the e-ph interaction in bulk.[15–17] In these calculations, the change of potential caused by a phonon is computed self-consistently from two structures, the perfect crystal and the crystal with a frozen phonon.[15] Thereafter, the calculations were performed using empirical pseudopotentials,[31,32] rigid-muffin-tin approximations,[33] and *ab initio* density functional theory (DFT)[16,19] along with phonon modes obtained from empirical valence force field models or first-principle linear response computations.

Despite the great success of the frozen-phonon approaches for the e-ph coupling in bulk, alloys, and graphene,[15–17,19,32] these methods have not been applied to study the e-ph coupling in colloidal semiconductor NCs. In this work, we extend the *ab initio* frozen-phonon approach to the computation of e-ph interaction in colloidal NCs. In the calculations discussed here, the electronic states and the potential perturbed through the vibrations are self-consistently calculated using *ab initio* DFT,[34] and the vibrational eigenmodes are obtained from DFT computation implemented with a finite-difference approach.[35]

A good agreement between the e-ph interaction matrix elements of small NC calculated using DFPT linear response and our frozen-phonon method confirms the applicability of the present approach. Moreover, our calculated e-ph transitions obey selection rules strictly. Furthermore, we extend the calculations for the e-ph interaction to silicon NCs with up to 1000 atoms and analyze the phonon-induced carrier relaxation based on the Wigner-Weisskopf approach. We also compare the intraband relaxation rate of silicon NC from our calculations to the experiments. We find the following: (i) The frozen-phonon approach can provide the e-ph interaction matrix elements of semiconductor NCs with up to one-thousand atoms at the DFPT linear-response level. (ii) The e-ph coupling strength is found to decrease with increasing cluster size. (iii) There is a decaying Rabi-like oscillation between the lowest unoccupied molecular orbit (LUMO) and the second conduction states of NC with emission and absorption of a phonon. (iv) The calculated intraband relaxation rate of silicon NCs is comparable to the experimental result, and this decay rate is determined by the phonon lifetime and the electron trapping time of NC surface states.

II. THEORETICAL METHOD

A. Electron-phonon interaction

Within the Born-Oppenheimer approximation, the many-body Hamiltonian of the NC is decomposed into an electronic part, an ionic part, and the coupling of the electron system with the lattice vibrations. The first two parts deal with the motions of electrons and ions separately while the third part describes the *electron-phonon interaction*. The e-ph interaction Hamiltonian can be expressed as a Taylor series expansion of the electronic potential:[14]

$$\Delta V^{\nu}(\boldsymbol{r},\boldsymbol{R}) = \sum_{I} \frac{\partial V}{\partial \boldsymbol{R}_I} \cdot \boldsymbol{u}_I^{\nu}, \tag{1}$$

where V is the electronic potential and $\boldsymbol{R}_I$ denotes the nuclear position of atom I. The displacement vector $\boldsymbol{u}_I^{\nu}$, which belongs to atom I and the vibrational eigenmode ν, can be written in terms of the normal coordinates Q^{ν},[13]

$$\boldsymbol{u}_I^{\nu} = \frac{1}{\sqrt{M_I}} Q^{\nu} \boldsymbol{X}_I^{\nu}, \tag{2}$$

with the occupation number representation,

$$Q^{\nu} = \sqrt{\frac{\hbar}{2\omega^{\nu}}}(a_{\nu}^{\dagger} + a_{\nu}),$$

where M_I is the mass of atom I, $\hbar$ is the reduced Planck constant, ω^{ν} is the frequency of the vibrational mode ν, $\boldsymbol{X}_I^{\nu}$ are the three components of the vibrational eigenmode belonging to atom I, and $a_{\nu}^{\dagger}$ and a_{ν} denote the creation and the annihilation operators of the ν-mode phonon.

According to Eqs. (1) and (2), the e-ph coupling matrix elements for the transition from the initial state $|\psi_n,0\rangle$ to the finial state $|\psi_m,1^{\nu}\rangle$ with emission of a ν-mode phonon has the form,

$$g^{\nu}(m,n) = \sum_{I} \sqrt{\frac{\hbar}{2M_I\omega^{\nu}}} \langle \psi_m,1^{\nu}| \frac{\partial V}{\partial \boldsymbol{R}_I} \cdot \boldsymbol{X}_I^{\nu}(a_{\nu}^{\dagger} + a_{\nu})|\psi_n,0\rangle, \tag{3}$$

where the polaron state $|\psi_m,i^{\nu}\rangle$ is composed of an electronic state $|\psi_m\rangle$ and a vibrational state $|i^{\nu}\rangle$.

B. Frozen-phonon approach

Based on the frozen-phonon approach for the e-ph coupling, the change of the potential caused by a phonon distortion in Eq. (3) is replaced by[15–17]

$$\sum_{I} \frac{\partial V}{\partial \boldsymbol{R}_I} \cdot \boldsymbol{X}_I^{\nu} \approx \frac{V_{\mathrm{scf}}^{\nu}(\boldsymbol{r}) - V_{\mathrm{scf}}^{0}(\boldsymbol{r})}{u^{\nu}}, \tag{4}$$

where $u^{\nu} = \sqrt{\sum_I \frac{1}{M_I} \boldsymbol{X}_I^{\nu 2}}$ is a scale describing effectively the frozen-phonon displacement caused by the lattice vibration, and $V_{\mathrm{scf}}^{\nu}(\boldsymbol{r})$ and $V_{\mathrm{scf}}^{0}(\boldsymbol{r})$ are the self-consistent potentials with and without the phonon distortion.[15–17]

In DFT, the self-consistent potential $V_{\mathrm{scf}}(\boldsymbol{r})$ has the form,[36]

$$V_{\mathrm{scf}}(\boldsymbol{r}) = V_{\mathrm{ion}}(\boldsymbol{r}) + e^2 \int \frac{\rho(\boldsymbol{r}')}{|\boldsymbol{r}-\boldsymbol{r}'|} d\boldsymbol{r}' + \frac{\delta E_{\mathrm{xc}}[\rho(\boldsymbol{r})]}{\delta \rho(\boldsymbol{r})}, \tag{5}$$

where the ionic potential $V_{\mathrm{ion}}(\boldsymbol{r})$ is typically decomposed into a local part $V_{\mathrm{ion}}^{\mathrm{loc}}(\boldsymbol{r})$ and a nonlocal part; the Hartree potential $e^2 \int \frac{\rho(\boldsymbol{r}')}{|\boldsymbol{r}-\boldsymbol{r}'|} d\boldsymbol{r}'$ and the exchange-correlation potential $\frac{\delta E_{\mathrm{xc}}[\rho(\boldsymbol{r})]}{\delta \rho(\boldsymbol{r})}$ are obtained self-consistently with $\rho(\boldsymbol{r}) = \sum_n^{\mathrm{occ}} |\psi_n(\boldsymbol{r})|^2$. The local part of the self-consistent potential $V_{\mathrm{scf}}^{\mathrm{loc}}(\boldsymbol{r})$, which includes the local ionic potential $V_{\mathrm{ion}}(\boldsymbol{r})$, the Hartree potential, and the exchange-correlation potential, is computed self-consistently using standard DFT. The nonlocal potential is calculated using the real space representation of the Kleinman-Bylander form:

$$\langle \boldsymbol{r}|V_{\mathrm{ion}}^{\mathrm{NL}}|\boldsymbol{r}'\rangle = \sum_{I,l,m} \frac{\langle \boldsymbol{r}|\delta V_l^I \phi_{lm}^I\rangle\langle \phi_{lm}^I \delta V_l^I|\boldsymbol{r}'\rangle}{\langle \phi_{lm}^I|\delta V_l^I|\phi_{lm}^I\rangle}, \tag{6}$$

where l and m label the angular and magnetic moments, $\phi_{lm}^I(\boldsymbol{r}-\boldsymbol{R}_I)$ are the pseudo-wave-functions centered on the atom position $\boldsymbol{R}_I$, and the potential $\delta V_l^I(|\boldsymbol{r}-\boldsymbol{R}_I|) = V_l^I(|\boldsymbol{r}-\boldsymbol{R}_I|) - V_{\mathrm{loc}}^I(|\boldsymbol{r}-\boldsymbol{R}_I|)$. In contrast to the local potential, the Kleinman-Bylander nonlocal potential in Eq. (6) is a projector. The contribution of the nonlocal potential to Eq. (4) takes the form,

$$\sum_I \sqrt{\frac{\hbar}{2M_I\omega^{\nu}}} \sum_{\boldsymbol{r},\boldsymbol{r}'} \left[\langle \psi_m|\boldsymbol{r}\rangle\langle \boldsymbol{r}|V_{\mathrm{ion}}^{\mathrm{NL},\nu}|\boldsymbol{r}'\rangle\langle \boldsymbol{r}'|\psi_n\rangle - \langle \psi_m|\boldsymbol{r}\rangle\langle \boldsymbol{r}|V_{\mathrm{ion}}^{\mathrm{NL},0}|\boldsymbol{r}'\rangle\langle \boldsymbol{r}'|\psi_n\rangle\right], \tag{7}$$

where $V_{\mathrm{ion}}^{\mathrm{NL},\nu}$ and $V_{\mathrm{ion}}^{\mathrm{NL},0}$ represent the nonlocal potential with and without phonon distortion.

Finally, using Eqs. (3)–(7) with the phonon distorted and undistorted atom positions $\{\boldsymbol{R}_I + \boldsymbol{X}_I^{\nu}/\sqrt{M_I}\}$ and $\{\boldsymbol{R}_I\}$, the e-ph interaction matrix elements of the NCs can be calculated at the *ab initio* level without additional parameters.

C. Electronic relaxation in nanoclusters

The Fermi golden rule is widely used in quantum physics to calculate the transition rate from one eigenstate into a *continuum* of eigenstates caused by a perturbation. Due to the discrete nature of the electronic *and* the vibrational states of QDs, the Fermi golden rule is inappropriate and the

Wigner-Weisskopf coupled-mode-equation approach is used to study the relaxation process.[37] In the Wigner-Weisskopf approach, the time evolution from an excited electronic state without phonon $|\psi_n,0\rangle$ to the ground state with the emission of a ν-mode phonon $|\psi_m,1^\nu\rangle$ can be expressed as

$$\Psi(t) = a(t)e^{-iE_nt/\hbar}|\psi_n,0\rangle + b(t)e^{-i(E_m/\hbar+\omega^\nu)t}|\psi_m,1^\nu\rangle, \quad (8)$$

where $a(t)$ and $b(t)$ are the amplitudes of the initial and the final states, and E_m and E_n are the electronic eigenvalues of the states $|\psi_m\rangle$ and $|\psi_n\rangle$, respectively. By inserting Eq. (8) into the time-dependent Schrödinger equation and introducing a decay channel between the polaron state $|\psi_m,1^\nu\rangle$ and the ground state $|\psi_0,0\rangle$, we obtain the coupled equations,

$$\begin{aligned}\frac{da(t)}{dt} &= -\frac{i}{\hbar}g^\nu(m,n)e^{i\Delta Et/\hbar}b(t),\\ \frac{db(t)}{dt} &= -\frac{i}{\hbar}g^{\nu*}(m,n)e^{-i\Delta Et/\hbar}a(t) - \gamma b(t),\end{aligned} \quad (9)$$

with the energy detuning $\Delta E = E_n - E_m - \hbar\omega^\nu$ and the decay rate γ. From Eq. (9) and the initial conditions $a(0) = 1$ and $b(0) = 0$, the occupation probability of the initial electronic state $P(t) = |a(t)|^2$ can be deduced analytically as shown in Ref. 38.

D. Computation details

We construct spherical NCs made of bulk silicon, centered on an atom. The resulting NCs have T_d point group symmetry. The dangling bonds are terminated by hydrogen atoms. The supercell is simple cubic with 3-Å space between the outermost atoms and the closest boundary. We use the local density approximation (LDA) and Trouiller-Martin norm-conserving pseudopotentials with an energy cutoff of 30 Ry. The forces are minimized to less than 3×10^{-6} a.u. under constrained symmetry. Based on the harmonic approximation of lattice dynamics, the phonon frequencies ω and the vibrational eigenmodes $\boldsymbol{U}$ are obtained by solving the eigenvalue equation,

$$\sum_{J=1}^{N}\frac{1}{\sqrt{M_IM_J}}\frac{\partial^2V}{\partial\boldsymbol{R}_I\partial\boldsymbol{R}_J}\boldsymbol{U}_J = \omega^2\boldsymbol{U}_I. \quad (10)$$

The vectors $\boldsymbol{X}_I^\nu$ in Eqs. (2)–(4) represent the three components that belong to atom I and the phonon mode ν from the $3N$ component eigenvector $\boldsymbol{U}_I$.[35,39] To analyze the eigenmodes in terms of bulk and surface contributions, we calculate the projection coefficients:

$$\alpha_{c,s}^\nu = \frac{\sum_{I=1}^{(N_c,N_s)}\left|\boldsymbol{X}_I^\nu\right|^2}{\sum_{I=1}^{N}\left|\boldsymbol{X}_I^\nu\right|^2}, \quad (11)$$

where N_c, N_s, and N are the core, surface, and total number of atoms. The surface atoms are defined as the atoms belonging to the outermost seven layers of the cluster (around 3-Å thick).

The electronic eigenstates $\psi_m(\boldsymbol{r})$ and $\psi_n(\boldsymbol{r})$, and the self-consistent local potential $V_{\rm scf}^{\rm loc}(\boldsymbol{r})$ are obtained by solving the Kohn-Sham equation self-consistently within DFT.[34] The l-dependent nonlocal pseudopotential δV_l^I and the pseudo-wave-function ϕ_{lm}^I are obtained from Trouiller-Martin norm-conserving pseudopotentials. The relaxed geometry of a $Si_{281}H_{172}$ NC with the wave functions of the LUMO (e_0) and the second conduction state (e_1) are shown in Fig. 1.

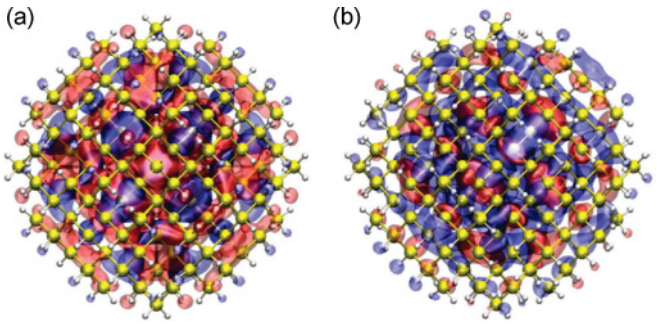

FIG. 1. (Color online) The wave functions of (a) e_0 and (b) e_1 states for $Si_{281}H_{172}$ nanocluster with isosurface corresponding to 75% of the maximum value. The colors blue and red give the phase of the wave functions. The silicon and passivating hydrogen atoms are represented by yellow and white spheres.

The implementation of the e-ph coupling matrix elements using the frozen-phonon approach involves the following steps. We optimize the geometry of the NC and calculate the corresponding electronic wave functions $\psi_{m(n)}(\mathbf{r})$, the unperturbed self-consistent potential $V_{\rm scf}^0(\mathbf{r})$, and the vibrational eigenmodes. The NC is then distorted by moving the atoms according to the atomic displacements given by the vibrational eigenvector. The phonon distorted potential $V_{\rm scf}^\nu(\mathbf{r})$ is calculated using this "frozen" geometry. With these quantities along with Eqs. (3)–(7), the e-ph coupling matrix elements can be obtained at the DFT level.

III. COMPARISON WITH DFPT

To verify the applicability of the present method to NCs, we calculate the e-ph interaction matrix elements for the e_1-to-e_0 transition in a $Si_{35}H_{36}$ cluster using both DFPT linear response[34] and our frozen-phonon approach. The vibrational density of states (DOS) is shown in Fig. 2(a) and is separated into contributions from silicon (thick black lines) and hydrogen (thin red lines). Figure 2(b) shows the e-ph interaction matrix elements $|g^\nu(m,n)|^2$ calculated using linear response[34] (black circles) and our frozen-phonon (red squares) approach. To give a further comparison between these two approaches, we plot the e-ph interaction matrix elements in a logarithmic scale in Fig. 2(c). We find agreement between both approaches with differences below 14% for the acoustic modes and 8% for the optical modes.

The discrepancy between the results obtained by the linear-response and frozen-phonon methods can be understood from the approximations used in both approaches. In the linear-response method, the "screened potential" ΔV^ν is calculated using a linear order approximation. In contrast to the linear-response approach, the frozen-phonon approach involves potential variations to all orders in the displacement. Furthermore, an average displacement of all the atoms in the cell is used as a scaling factor in the frozen-phonon approach following the original idea.[15–17] In the case of long wavelength acoustic phonons, the atomic displacements correspond to a macroscopic distortion of the lattice and a macroscopic strain tensor is needed to describe the electron-acoustic phonon

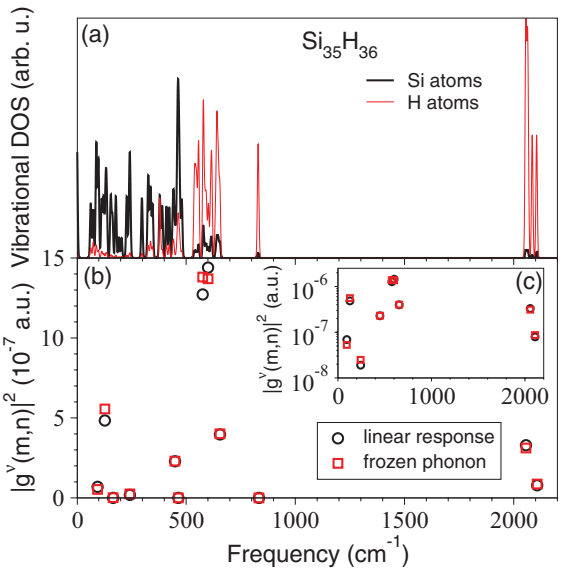

FIG. 2. (Color online) (a) Vibrational DOS of $Si_{35}H_{36}$ NCs contributed by Si atoms [thick (black) lines] and H atoms [thin (red) lines] with a Gaussian broadening of 0.8 cm^{-1}, (b) e-ph matrix elements for e_0 and e_1 states obtained from linear-response calculations (circles) and our frozen-phonon approach (squares), and (c) same as (b) but using logarithmic scale.

interaction.[14] Unlike the acoustic modes, the optical modes can be regarded as microscopic distortions.[14] Therefore, the errors introduced by the average displacement in the frozen-phonon approach for the electron-acoustic phonon interactions may be larger than those for the optical ones.

IV. SIZE DEPENDENCE OF THE ELECTRON-PHONON INTERACTION

Although the e-ph interaction of semiconductor NCs have been studied for decades from both theoretical and experimental aspects,[40–44] the size effects on the e-ph interaction are still somewhat controversial. Based on different theoretical approaches and experimental measurements, an increase,[43,44] decrease,[40,42] or size independence[41] of e-ph interaction with decreasing NC size have been reported. In order to study the size effects on the e-ph interaction strength, we plot the e-ph interaction matrix elements for e_1-to-e_0 transition via the bulklike acoustic (black circles) and optical (red squares) phonon modes of $Si_{281}H_{172}$ (R = 11.9 Å), $Si_{633}H_{300}$ (R = 15.7 Å), and $Si_{705}H_{300}$ (R = 16.3 Å) NCs in Fig. 3. To keep the comparability of e-ph matrix elements of different NCs, we choose the phonon modes with the same vibrational character of each NC. From Fig. 3, we see that the e-ph coupling strengths are strongly dependent on cluster size with a dropping of two orders of magnitude from the smallest to the largest NCs we studied. Furthermore, the coupling strengths of the electron-acoustic phonon are stronger than those of the electron-optical phonon. These results agree with a recent theoretical study on e-ph coupling in CdSe NCs from the atomistic phonon model.[44]

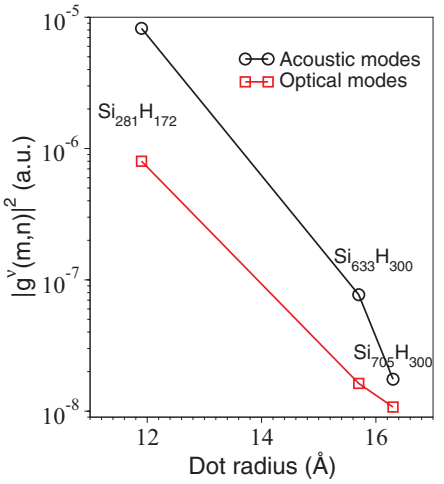

FIG. 3. (Color online) Size-dependent e-ph matrix elements for e_1-e_0 transition of Si NCs via acoustic (black circles) and optical (red squares) phonon.

V. ULTRAFAST PROCESS VIA ELECTRON-PHONON INTERACTION

After looking at the applicability of our frozen-phonon approach, we now apply this method to study the e_1-to-e_0 transition of $Si_{281}H_{172}$ and $Si_{705}H_{300}$ NCs. In this paper, we calculate the e-ph interaction matrix elements $|g^{\nu}(m,n)|^2$ using our frozen-phonon method and employ the Wigner-Weisskopf approach[37,38] to analyze the transition between the discrete energy levels. Different aspects of the results are summarized in Fig. 4.

In Fig. 4(a), we plot the conduction band states of a $Si_{281}H_{172}$ NC, where the LUMO state e_0 and the second conduction band state (or electron state) e_1 belong to the Γ_1 and Γ_4 point group representations, respectively, and are energetically split by 49.9 meV (402.4 cm^{-1}). The vibrational DOS of the $Si_{281}H_{172}$ NC contributed by the core (thick black line) and surface (thin red line) atoms are given in Fig. 4(b). The arrow indicates the e_1-to-e_0 energy spacing $\Delta = E_1 - E_0$. To understand the e_1-to-e_0 transition process via e-ph interaction, we plot in Fig. 4(c) the energy level system schematically. Specifically, we consider (i) an electron relaxation from the second electron state $|e_1,0\rangle$ to a polaron state $|e_0,1^{\nu}\rangle$ via emission/creation of a ν-mode phonon; (ii) the reverse process (i.e., an electron transition from the LUMO to the e_1 state via absorption/annihilation of a ν-mode phonon), and (iii) the decay of the phonon part of the polaron state $|e_0,1^{\nu}\rangle$ to $|e_0,0\rangle$ given by the phonon lifetime $\tau_{\rm ph}$.

In Fig. 4(d), we give the numerical values of the e-ph matrix elements for vibrational modes energetically close (<4 cm^{-1}, 0.5 meV) to the electronic energy splitting Δ. We can see that the numerical values of the e-ph matrix elements for vibrations with Γ_4 symmetry are in the range of 10^{-6} a.u. while those for the other symmetry are zero. Selection rules for the e-ph interaction can be understood as follows. In the e_1-to-e_0 transition process, the initial state (e_1) belongs to the Γ_4 point group representation and the final state (e_0) has Γ_1 symmetry. This transition will be achieved only when the vibrations can transfer the wave-function symmetry from the Γ_4 into the Γ_1 point group representations. An analysis of the point group

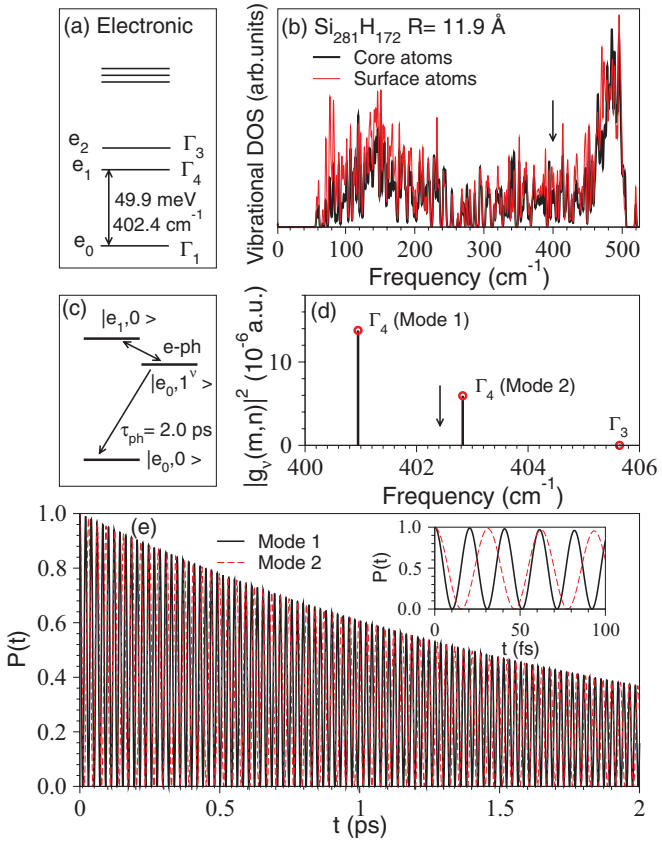

FIG. 4. (Color online) (a) Electronic levels of $Si_{281}H_{172}$ nanocluster, (b) vibrational DOS of $Si_{281}H_{172}$ NC contributed by core (thick black) and surface atoms [thin red (gray)] with a broadening of 0.8 cm^{-1}, (c) schematic showing the electronic transition process via e-ph interaction, (d) e-ph matric elements for the interaction between e_0, e_1 states and the vibrations with the phonon energy $\hbar\omega^{\nu}$ around the electron energy level spacing $E_1 - E_0$, and (e) probability of e_1 state interacted by mode 1 (solid lines) and mode 2 (dashed lines) vibrations. The inset shows the oscillation of $P(t)$ within 100 fs.

symmetry reveals that only phonons with Γ_4 symmetry are active for this e_1-to-e_0 transition.[14]

Following the discussion on the e-ph interaction matrix elements, we now focus on the interesting time-dependent occupation probability of the initial electronic state $P(t)$ based on the Wigner-Weisskopf approach. We plot in Fig. 4(e) the probability of finding the electron in the initial state caused by the e-ph interaction for the phonon modes 1 and 2 with an energy detuning of 0.2 and 0.05 meV, respectively. The phonon lifetime τ_{ph} is taken as 2.0 ps according to experimental results on bulk silicon.[45] In Fig. 4(e), we observe that the probability of finding the electron in the initial state decays with a Rabi-like oscillation. In addition, we note that the oscillation period of mode 1 is shorter than that of mode 2 from the inset of the figure. Following Fig. 4(c), we see that the electron in state e_1 cyclically emits a phonon and reabsorbs it, which results in a repeated energy exchange between the electron and the vibration. This repeated process decays with the decay rate of the phonon mode. As a result, the excited electron finally returns to the ground state while the energy has been transferred into low frequency vibrations. We conclude that the ultrafast oscillations reflect the e-ph interaction process. The

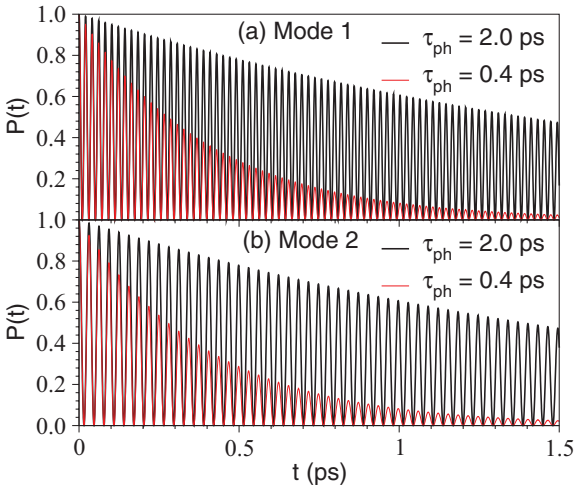

FIG. 5. (Color online) Probability of the initial electron state $P(t)$ for (a) mode 1 and (b) mode 2 of $Si_{281}H_{172}$ NC. The phonon lifetimes are 2.0 (thick black) and 0.4 ps [thin red (gray)].

shorter oscillation period observed for mode 1 is a consequence of the stronger e-ph interaction for this specific mode. To understand the effects of phonon lifetime on the e_1-to-e_0 transition process, we plot in Fig. 5 the probability of the e_1 state for modes 1 (a) and 2 (b) with a phonon lifetime of 2.0 (thick black) and 0.4 ps (thin red).[45] We see that the envelope function of $P(t)$, which retains the same oscillation period for both modes, decays according to the phonon lifetime.

After analyzing the e_1-to-e_0 transition process of $Si_{281}H_{172}$ NC via the e-ph interaction, we now extend our calculation to a larger NC. The vibrational DOS, the e-ph matrix elements for the e_1-to-e_0 transition along with the probability of finding the electron in the e_1 state for a $Si_{705}H_{300}$ NC, are given in Figs. 6(a)–6(c). From Figs. 6(a) and 6(b), we see that the electron energy level spacing between the e_1 and e_0 states of $Si_{705}H_{300}$ NC is 6.5 meV (52.4 cm^{-1}), which corresponds to the phonon energy of the surface acoustic modes. In Fig. 6(b), we give the results of the e-ph matrix elements for vibrational modes with energy detuning less than 0.2 meV. As in the previous case, the e-ph transitions obey section rules (i.e., the e-ph matrix element for vibration with Γ_4 symmetry is in the range of 10^{-6} a.u. while that for the other symmetries is zero). The occupation probability of the electron in state e_1 for the $Si_{705}H_{300}$ NC is plotted in Fig. 6(c) with τ_{ph} as 0.4 and 2.0 ps and shows the same characteristics as for the $Si_{281}H_{172}$ NC.

VI. COMPARISON WITH EXPERIMENTS

Experimentally, the intraband $1P$-to-$1S$ relaxation process in semiconductor NCs is mostly explored via femtosecond pump-probe measurements.[46–50] In experiments, electrons and holes are pumped into the excited states ($1P$) by an ultrafast laser and thereafter the electrons decay into the ground state ($1S$) rapidly. After this fast relaxation inside the NC, the carriers recombine radiatively or become trapped at the surface of the NC.[46–50] To understand the $1P$-to-$1S$ relaxation process, we plot the probability of the time-dependent $1P$-to-$1S$ transition process via phonon mode 2 ($\tau_{ph} = 2.0$ ps)

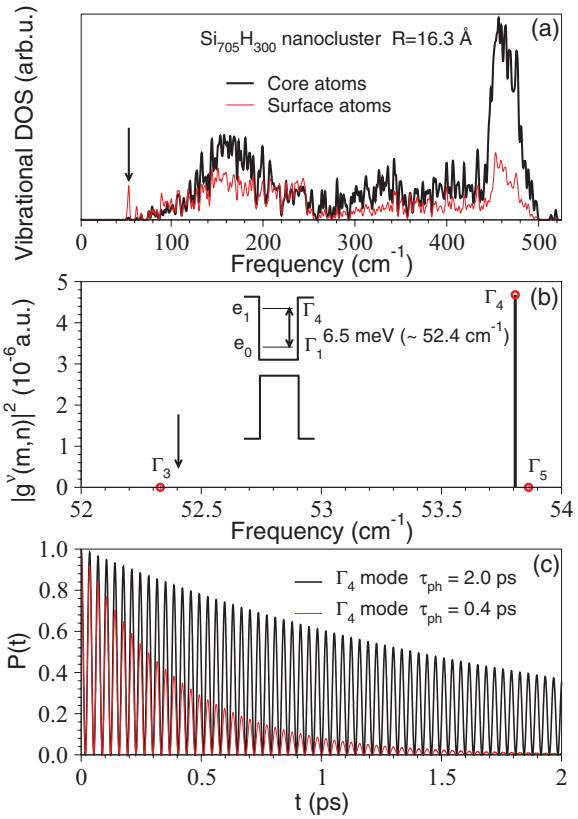

FIG. 6. (Color online) (a) Vibrational DOS of $Si_{705}H_{300}$ NC contributed by core (thick black) and surface atoms [thin red (gray)] with a broadening of 0.8 cm^{-1}, (b) e-ph matrix elements for the interaction between e_0, e_1 states and the vibrations with the phonon energy $\hbar\omega^{\nu}$ around the electron energy level spacing $E_1 - E_0$, and (c) probability of e_1 state interacted by vibration with Γ_4 symmetry with phonon lifetime as 2.0 and 0.4 ps.

in Figs. 7(a) and 7(b) with surface trapping times τ_{tr} of 0.4 and 0.6 ps,[49] respectively. In this case, the total decay time $\tau_{tot} = 1/(\tau_{ph}^{-1} + \tau_{tr}^{-1})$. From Fig. 7, we see a decaying oscillation of the electron between the $1P$ and $1S$ states with a period of tens of femtoseconds. In experiments with limited time resolution, the envelope function instead of the oscillations will be measured. Using an exponential fit to the envelope function, we find a lifetime of 0.34–0.45 ps for the intraband relaxation, which is comparable to experiments.[48] Similar to the discussion in Sec. IV, we attribute the decay of the envelope function to the effects of both the phonon lifetime and the electron trapping time of the surface states.

VII. SUMMARY

In summary, we have given an *ab initio* DFT self-consistent approach to calculate the e-ph interaction matrix elements of

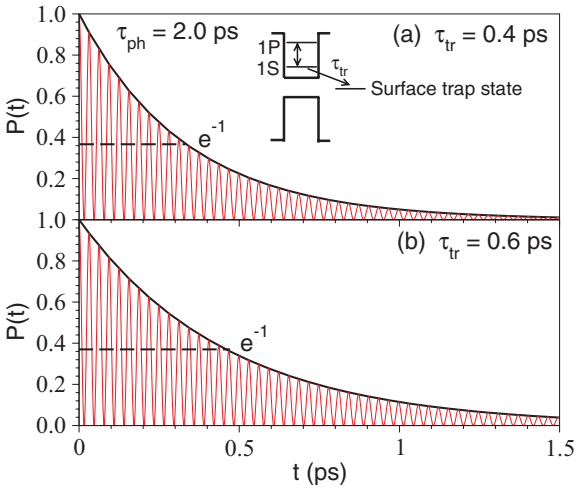

FIG. 7. (Color online) Probability of $1P$ state during the $1P$-to-$1S$ transition process caused by phonon mode 2 with carrier trapping times in the NC surface state τ_{tr} (a) 0.4 and (b) 0.6 ps. Scheme of this transition process is given in the insert of (a).

semiconductor NCs based on the frozen-phonon approach. We find a good agreement between the results of our approach and *ab initio* DFPT linear response. The present approach allows us to compute the e-ph matrix elements of NCs with up to 1000 atoms at the DFT level and paves the way to study the dynamical processes of nanostructures. Based on the frozen-phonon calculations, we find that the e-ph interaction strength is strongly dependent on the cluster size and there is a dropping of two orders of coupling strength magnitude with dot radius from 12 to 16 Å. We further calculate the e_1-to-e_0 transition processes of $Si_{281}H_{172}$ and $Si_{705}H_{300}$ NCs via e-ph interaction and analyze the relaxation processes between the discrete electron levels using the Wigner-Weisskopf approach. We observe a decaying Rabi-like oscillation in our two-state quantum system driven by the emission and absorption of a phonon and notice that the oscillation period is determined by the e-ph interaction. The $1P$-to-$1S$ intraband relaxation rate of silicon NCs is calculated using our approach and compared to the experimental results. We note that the fast intraband relaxation rate is determined by the phonon lifetime and the electron trapping time of the NC surface states.

ACKNOWLEDGMENTS

We thank Dr. Pierre-Yves Prodhomme for helpful discussions and acknowledge financial support from the Marie Curie Reintegration Grant and the BMBF (QuaHL-Rep, Contract No. 01BQ1034). Most of the simulations were preformed on the national supercomputer NEC Nehalem Cluster at the High Performance Computing Center Stuttgart (HLRS).

*g.bester@fkf.mpg.de

[1] P. Alivisatos, Nat. Biotechnol. **22**, 47 (2004).
[2] V. I. Klimov, S. A. Ivanov, J. Nanda, M. Achermann, I. Bezel, J. A. McGuire, and A. Piryatinski, Nature (London) **447**, 441 (2007).
[3] R. M. Kraus, P. G. Lagoudakis, A. L. Rogach, D. V. Talapin, H. Weller, J. M. Lupton, and J. Feldmann, Phys. Rev. Lett. **98**, 017401 (2007).
[4] J. M. Harbold and F. W. Wise, Phys. Rev. B **76**, 125304 (2007).

[5]U. Banin, Nat. Photonics **2**, 209 (2008).
[6]A. L. Rogach, N. Gaponik, J. M. Lupton, C. Bertoni, D. E. Gallardo, S. Dunn, N. L. Pira, M. Paderi, P. Repetto, S. G. Romanov, C. O'Dwyer, C. M. S. Torres, and A. Eychmueller, Angew. Chem., Int. Ed. Engl. **47**, 6538 (2008).
[7]A. Pandey and P. Guyot-Sionnest, Science **322**, 929 (2008).
[8]G. D. Scholes, Adv. Funct. Mater. **18**, 1157 (2008).
[9]D. V. Talapin, J. Lee, M. V. Kovalenko, and E. V. Shevchenko, Chem. Rev. **110**, 389 (2010).
[10]S. V. Kilina, D. S. Kilin, and O. V. Prezhdo, ACS Nano **3**, 93 (2009).
[11]V. M. Huxter and G. D. Scholes, J. Chem. Phys. **132**, 104506 (2010).
[12]P. Han and G. Bester, Phys. Rev. B **83**, 174304 (2011).
[13]O. Madelung, *Introduction to Solid-State Theory* (Springer Press, Berlin, 1996).
[14]P. Y. Yu and M. Cardona, *Fundamentals of Semiconductors* (Springer Press, Berlin, 2010).
[15]M. M. Dacorogna, M. L. Cohen, and P. K. Lam, Phys. Rev. Lett. **55**, 837 (1985).
[16]P. K. Lam, M. M. Dacorogna, and M. L. Cohen, Phys. Rev. B **34**, 5065 (1986).
[17]K. J. Chang and M. L. Cohen, Phys. Rev. B **34**, 4552 (1986).
[18]F. Murphy-Armando and S. Fahy, Phys. Rev. B **78**, 035202 (2008).
[19]J. A. Yan, W. Y. Ruan, and M. Y. Chou, Phys. Rev. B **79**, 115443 (2009).
[20]S. Y. Savrasov, D. Y. Savrasov, and O. K. Andersen, Phys. Rev. Lett. **72**, 372 (1994).
[21]F. Mauri, O. Zakharov, S. de Gironcoli, S. G. Louie, and M. L. Cohen, Phys. Rev. Lett. **77**, 1151 (1996).
[22]A. Y. Liu and A. A. Quong, Phys. Rev. B **53**, R7575 (1996).
[23]R. Bauer, A. Schmid, P. Pavone, and D. Strauch, Phys. Rev. B **57**, 11276 (1998).
[24]J. Sjakste, N. Vast, and V. Tyuterev, Phys. Rev. Lett. **99**, 236405 (2007).
[25]F. Giustino, M. L. Cohen, and S. G. Louie, Phys. Rev. B **76**, 165108 (2007).
[26]J. Gavartin and A. Shluger, Phys. Status Solidi C **3**, 3382 (2006).
[27]D. Muñoz Ramo, A. L. Shluger, J. L. Gavartin, and G. Bersuker, Phys. Rev. Lett. **99**, 155504 (2007).
[28]D. T. Devreese and P. van Camp, *Electronic Structure, Dynamics, and Quantum Structural Properties of Condensed Matter* (Springer Press, New York, 1985).
[29]W. Frank, C. Elsässer, and M. Fähnle, Phys. Rev. Lett. **74**, 1791 (1995).
[30]S. Baroni, S. de Gironcoli, A. D. Corso, and P. Giannozzi, Rev. Mod. Phys. **73**, 515 (2001).
[31]P. B. Allen and M. L. Cohen, Phys. Rev. **187**, 525 (1969).
[32]S. Zollner, S. Gopalan, and M. Cardona, J. Appl. Phys. **68**, 1682 (1990).
[33]D. A. Papaconstantopoulos, L. L. Boyer, B. M. Klein, A. R. Williams, V. L. Morruzzi, and J. F. Janak, Phys. Rev. B **15**, 4221 (1977).
[34]P. Giannozzi *et al*., J. Phys.: Condens. Matter. **21**, 395502 (2009).
[35]The CPMD consortium page, coordinated by M. Parrinello and W. Andreoni, copyright IBM Corp 1990–2008, copyright MPI für Festkörperforschung Stuttgart 1997–2001 [http://www.cpmd.org].
[36]R. M. Martin, *Electronic Structure Basic Theory and Practical Methods* (Cambridge University Press, Cambridge, 2004).
[37]V. Weisskopf and E. Wigner, Z. Phys. **63**, 54 (1930).
[38]X. Q. Li, H. Nakayama, and Y. Arakawa, Phys. Rev. B **59**, 5069 (1999).
[39]S. Wei and M. Y. Chou, Phys. Rev. Lett. **69**, 2799 (1992).
[40]S. Schmitt-Rink, D. A. B. Miller, and D. S. Chemla, Phys. Rev. B **35**, 8113 (1987).
[41]M. C. Klein, F. Hache, D. Ricard, and C. Flytzanis, Phys. Rev. B **42**, 11123 (1990).
[42]A. M. dePaula, L. C. Barbosa, C. H. B. Cruz, O. L. Alves, J. A. Sanjurjo, and C. L. Cesar, Appl. Phys. Lett. **69**, 357 (1996).
[43]G. Scamarcio, V. Spagnolo, G. Ventruti, M. Lugará, and G. C. Righini, Phys. Rev. B **53**, R10489 (1996).
[44]A. M. Kelley, ACS Nano **5**, 5254 (2011).
[45]J. J. Letcher, K. Kang, D. G. Cahill, and D. D. Dlott, Appl. Phys. Lett. **90**, 252104 (2007).
[46]V. I. Klimov and D. W. McBranch, Phys. Rev. Lett. **80**, 4028 (1998).
[47]P. Guyot-Sionnest, M. Shim, C. Matranga, and M. Hines, Phys. Rev. B **60**, R2181 (1999).
[48]M. Sykora, L. Mangolini, R. D. Schaller, U. Kortshagen, D. Jurbergs, and V. I. Klimov, Phys. Rev. Lett. **100**, 067401 (2008).
[49]K. Zidek, F. Trojanek, P. Maly, L. Ondic, I. Pelant, K. Dohnalova, L. Siller, R. Little, and B. R. Horrocks, Opt. Express **18**, 25241 (2010).
[50]K. Zidek, I. Pelant, F. Trojanek, P. Maly, P. Gilliot, B. Hönerlage, J. Oberle, L. Siller, R. Little, and B. R. Horrocks, Phys. Rev. B **84**, 085321 (2011).